

## Light Ion Beam Transport Research at NRL

D. D. Hinshelwood, J. R. Boller, G. Cooperstein, R. C. Fisher,<sup>1</sup> J. M. Greenly,<sup>2</sup>  
T. G. Jones, D. Mosher, J. M. Neri, W. A. Noonan,<sup>5</sup> B. V. Oliver, C. L. Olson,<sup>3</sup>  
P. F. Ottinger, D. V. Rose,<sup>1</sup> S. J. Stephanakis, D. R. Welch,<sup>4</sup> and F. C. Young

*Plasma Physics Division, Naval Research Laboratory,  
Washington DC, 20375 USA*

<sup>1</sup>*JAYCOR, Vienna VA, 22181 USA*

<sup>2</sup>*Cornell University, Ithaca NY, 14853 USA*

<sup>3</sup>*Sandia National Laboratories, Albuquerque NM 87185 USA*

<sup>4</sup>*Mission Research Corporation, Albuquerque NM 87106 USA*

<sup>5</sup>*University of Maryland, College Park, MD 20742 USA*

### Abstract

Transport of light ion beams through low-pressure background gas is under investigation at NRL in support of the light-ion ICF program at Sandia National Laboratories. Scaling experiments and the field solver/orbit code ATHETA have been used to design and construct a focusing, extraction applied-B diode for transport experiments. We have developed an active anode source to provide a high proton fraction in the ion beam and a fast ion turn-on time. A very sensitive Zeeman diagnostic is being developed to determine the net current distribution in the beam/transport system. Both analytical and numerical techniques using several codes are being applied to transport modeling, leading to the capability of full system studies.

### Introduction

In a light-ion-beam inertial-confinement-fusion (ICF) reactor, transport over 4 meters from the diode to the target is needed to provide power compression by time-of-flight bunching and for standoff of the diode hardware from the target [1,2]. Two schemes are studied at present, neither of which involves any hardware in the reactor chamber: (1) ballistic transport with solenoidal lens focusing (BTSF), where an auxiliary field just outside the chamber, and the diode field, combine to form an achromatic lens pair that focuses the ion beam onto the target; and (2) self-pinched transport (SPT), where the beam is focused into a region of low-pressure gas, where incomplete current neutralization provides a net current that confines the ion beam in a narrow channel to the target. This approach is particularly exciting because the predicted net currents would allow a shorter focal length than with BTSF, and thus an increased beam microdivergence. Microdivergence reduction is a major, ongoing problem of diode research, and so transport research has great leverage for the ICF program. SPT of ICF-parameter beams requires net currents of at least a few percent, while BTSF of these beams requires net currents of at most a tenth of a percent (larger net currents for BTSF act like a distributed lens which must be accommodated for in the transport system). Therefore, the physics of gas breakdown and conductivity growth is crucial to both schemes. While we are studying both transport schemes, our primary effort at present is directed toward self-pinched transport of proton beams produced by an applied-B diode on the Gamble II generator.

### Self-pinched transport experiment

In designing a self-pinched transport experiment, we want to choose the system parameters to minimize the net current fraction needed to confine the beam. At the same time, we want the

injected proton current to be as large as possible to maximize our relevance to ICF. For a given channel radius, the net current fraction  $I_c/I_p$  and proton current  $I_p$  are given by:

$$\frac{I_c}{I_p} \propto \frac{\Theta_\mu^2 D^2}{\eta V f_p} \qquad I_p \propto \frac{V^{3/2} \eta R^2 f_p}{D^2}$$

where  $\Theta_\mu$ ,  $D$ ,  $\eta$ ,  $V$ ,  $f_p$ , and  $R$  refer to the beam microdivergence, diode gap, ion current enhancement in the diode (relative to the Child-Langmuir value), voltage, proton fraction, and diode outer radius, respectively. Thus we want a small microdivergence, high voltage, large radius, high proton fraction, high enhancement, and small gap. Since applied-B diode behavior degrades as the enhancement is raised or the gap reduced, it is necessary to see how far these parameters can be pushed.

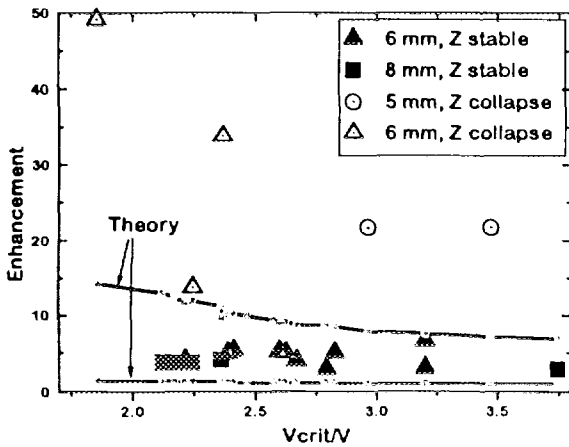


Figure 1: Summary of small-diode data

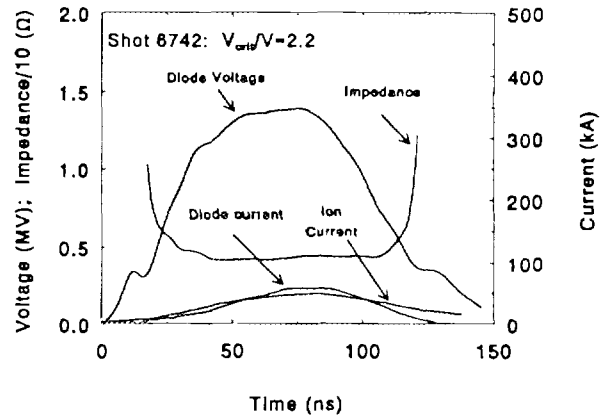


Figure 2: Typical shot at moderate enhancement

Results obtained with a small-area ( $50 \text{ cm}^2$ ) applied-B diode guide our design. In Fig. 1, the observed ion current enhancement is plotted as a function of  $V_{crit}/V$ , which is a measure of the applied field strength. The shots are divided into those with stable impedance histories and those which exhibit rapid impedance collapse. The lines show the range of enhancement predicted by Desjarlais' theory [3] in the absence of anode plasma expansion. As the applied field is reduced to raise the enhancement, or as the gap is reduced below 6 mm, we observe impedance collapse (there are many more "collapse" points beyond the upper left of this graph) and high enhancement that is indicative of rapid anode plasma expansion.

Figure 2 shows data from a typical shot with moderate enhancement, showing stable impedance and very high ion current efficiency. The microdivergence is about 20 mrad, but the proton fraction is about 50%, and the resulting 25-kA proton current is too low to be interesting. The current can be scaled up by increasing the diode area and voltage.

The small-diode results point to a minimum gap of 6 mm, an enhancement of 5, and a microdivergence of 20 mrad. Gamble II constraints limit the voltage to 1.5 MV and the radius to 10.5 cm. Relevance to ICF dictates a maximum channel radius of 2 cm. This specifies the diode design, with an expected ion current of 200 kA. The 20 mrad microdivergence dictates a 70-cm focal length, and the resulting confinement current is about 40 kA. Therefore, with a 50% proton fraction, a 40% net current fraction will be needed. Numerical simulations predict

this fraction to be achievable, but we would like to decrease it by boosting the proton content of our beam.

Design of this shallow-focusing diode is carried out using the Sandia field-solver and orbit code ATHETA [4]. As seen in Fig. 3a for a simple spherically-focusing anode, the applied and self fields combine to overfocus ions emitted from outer radii and defocus ions emitted from the inner radii. The former can be corrected by shaping the anode, but the latter can only be fixed by moving the emission surface to larger radius and moving the inner coil to smaller radius. Doing so increases the mechanical stress on the inner coil. This is compensated for by doubling the coil width. After iteratively tuning the anode shape, good focusing is recovered, as seen in Fig 3b.

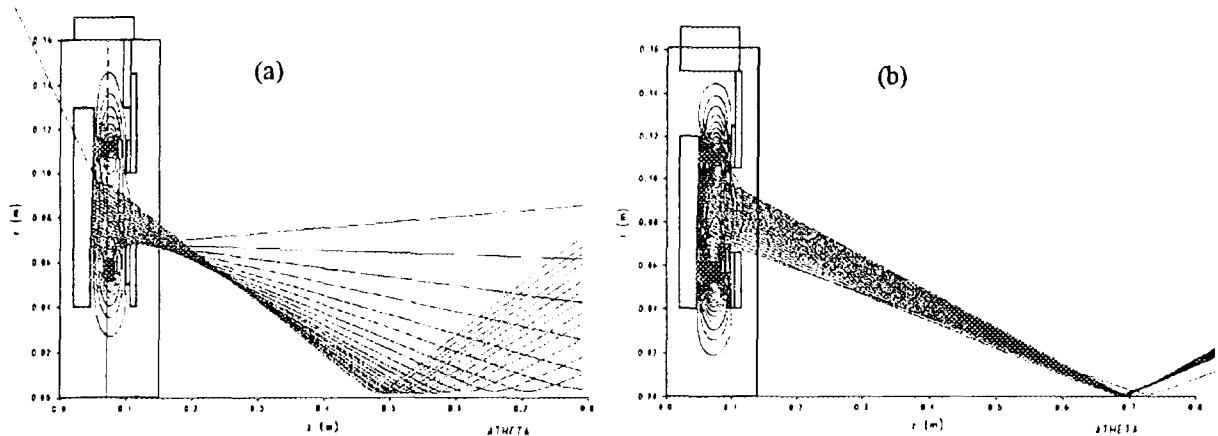


Figure 3: (left) ATHETA predictions for spherical anode; (right) predictions for shaped convex anode.

These calculations neglect field diffusion into the metal, and anode plasma expansion. When both are included, ions are no longer emitted from a zero flux surface. The resulting angular momentum prevents focusing. The solution is to pulse the coils first with a slow, low-amplitude reverse current, producing a field whose diffusion cancels that of the main field. When field diffusion and an assumed 1-mm anode plasma expansion are both taken into account, a proper choice of counterpulse field allows us to recover ATHETA predictions very similar to those in the right of Fig. 3.

A new diode has been constructed based on the above analysis and is being tested on the Gamble II generator. The applied field is 7.5 T in the gap and 12 T at the inner coil surface, giving a large but tolerable mechanical stress. Because the diode operates at a higher impedance than the generator, a parallel, blade load located upstream of the diode is used to shed the excess generator current.

#### Active anode source

An EMFAPS active anode source, based on those used at Cornell and the Karlsruhe Research Center (FZK) [5], will be used to improve the proton fraction and ion turn-on time. This consists of a thin layer of metal deposited on a dielectric substrate. A fast current pulse desorbs and ionizes adsorbed gas, resulting in a thin layer of plasma conformal to the anode. In the Cornell and FZK experiments, an opening switch diverts the early generator current through the foil. To improve controllability, we drive the foil with an external pulser. This

source has increased the proton fraction in our small-diode experiments. The drive system has been upgraded for the new diode. A low-inductance ( $\sim 2$  nH), low-jitter ( $\sim 2$  ns) solid foil switch, triggered by the generator, switches a small water line into six striplines that carry current through the transit-time isolator to the foil. A small surface-flashover switch located just before the foil blocks the water-line prepulse. This system provides a 120-kA, 20-ns foil current pulse with a peak  $dI/dt$  of over 10 kA/ns. Bench testing of the source for the new diode has just begun. We see uniform light emission from the foil breakdown, with no significant arcing or filamentation.

### Beam magnetic field profile measurement

To study beam current neutralization we need to know the magnetic field profile in the beam. Measurement of Zeeman splitting is made difficult by the small shifts involved: for the self-pinched case, the splitting is  $\sim 0.01 \text{ \AA}$ , below the resolution of most stigmatic instruments, and for the ballistic case, it is  $\sim 0.001 \text{ \AA}$ , within the Doppler profile. The solution is to use polarization selection with differential detection [6]. The approaches used for the two transport schemes are shown in Fig. 4. The narrow-band pump beam is directed across a diameter of the ion beam, in an appropriately seeded gas, imaging the transverse fluorescence. This gives spatial resolution and results in always looking along the field, where the two Zeeman components have opposite circular polarization. They are separated and differentially detected. For the low-field case, we tune the pump to the wings of the Doppler profile. For the high-field case, where the splitting exceeds the Doppler width, we plan to pump the  $m=0$  excited state, and then insert a monochromator, tuned so that the lines are at the edge of the response curve. In both cases, the differential signal will be related to the Zeeman splitting. Atomic physics and technological considerations point to the use of barium for the low-field case and samarium for the high-field case. We have demonstrated a proof-of-principle of the low-field technique on the bench, using Helmholtz coils to provide the field. We have achieved 20-Gauss resolution, as shown in Fig. 5. The next step will be to repeat this for the high-field technique, and then address the issues of fielding this diagnostic in the pulsed-power environment.

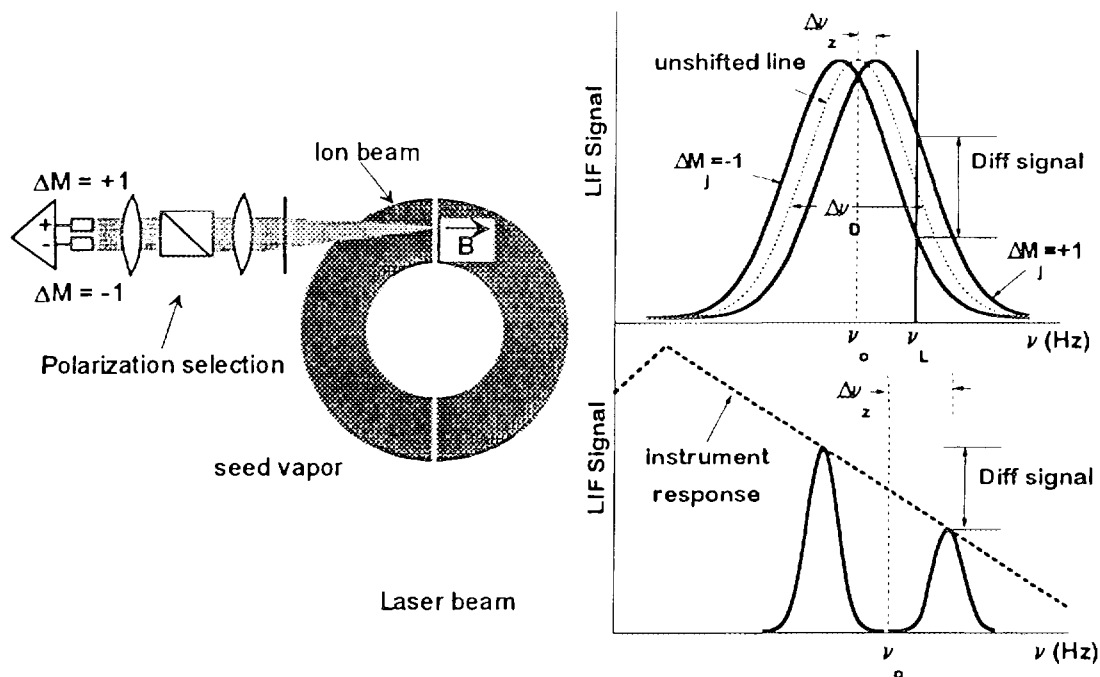


Figure 4: (left) Zeeman diagnostic; (top right) scheme for BTSF; (bottom right) scheme for SPT.

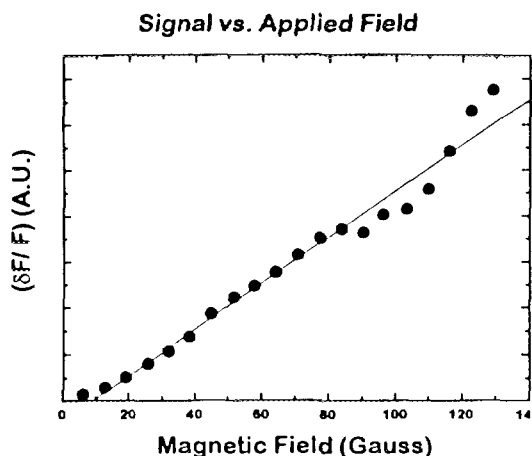


Figure 5: Bench test of Zeeman diagnostic

Gas	$t_{th}$ (ns)	$t_b$ (ns)	$t_r$ (ns)
GII - He	0.23	1.30	85.0
GII - N	0.05	0.50	5.0
GII - Ar	0.03	0.27	4.5
ICF - He	0.04	0.30	9.0

Table 1: Gas breakdown timescales

### Gas breakdown and conductivity growth theory

We are using many theoretical tools to study gas breakdown and conductivity growth: a zero-D code and analytic modeling [7] to get scaling laws; a 1-D PIC code with a detailed atomic physics treatment to model the early-time phenomena, and the multidimensional hybrid codes IPROP (3-D) [8] and Solenz (21/2-D) [9]. The use of these models is contributing to a complete understanding of gas breakdown.

IPROP, with its fluid treatment of cold electrons and PIC treatment of fast particles, has made encouraging predictions for self-pinched transport [8]. For conditions relevant to the Sandia SABRE generator, net current fractions of up to 50% in low-pressure argon are predicted. Zero-D calculations illustrate the relevance of the Gamble II experiments to ICF. Calculation of the energy input to the gas is fairly straightforward; its equipartition between ionization and electron temperature is key to current neutralization. We find 3 important timescales - energy input  $t_{th}$ , impact ionization  $t_b$ , and conductivity growth  $t_r$ . These timescales are given in Table 1 for different gases at Gamble II parameters and for helium at ICF parameters.

There are two questions in evaluating self-pinched transport: (1) can the required net currents be obtained? and (2) given these net currents, how well will the ion beam propagate? The first can be addressed by using the heavier gases, which have timescales similar to those under ICF conditions. The second can be addressed by using helium, which should provide the larger net current fraction needed for confinement under Gamble II conditions.

The zero-D code is being used to model earlier transport experiments on Gamble II, calculating the net current fraction, electron density, and temperature for different gases under these parameters. The electron density was measured interferometrically in the experiment. Theory gives good agreement for He and N but overpredicts the density by over a factor of two for Ar. We speculate that the electron tail distribution in the experiment may differ from the Maxwellian assumed in the code. Diagnostics of the electron tail, where ionization occurs, are necessary. Actinometry using emission from highly excited states of tracer elements is one possibility.

### Operational windows for transport systems

In addition to gas breakdown calculations, our theory effort is directed toward other transport issues, such as instabilities (filamentation and two-stream) and transport efficiency (including the effects of beam energy loss, focus sweep from voltage variations, and module packing constraints). Using system design parameters such as time-of-flight bunching, background gas species/pressure, etc., operational windows for stable and efficient transport can be determined. For example, preliminary results for the BTSF scheme using baseline ICF design parameters indicate that it may be difficult to avoid filamentation growth in the transport region between the diode and the solenoidal lens. These results may be different for other parameter sets, and this complete system modeling is continuing.

### Summary

In conclusion, the applied-B diode, active anode source, and theoretical tools are ready for self-pinch transport experiments that will begin soon. Future work will center on refining both the diagnostics - the very sensitive Zeeman diagnostic, emission studies of the electron distribution, and measurement of the electron density using a highly sensitive ( $10^{-4}$  fringe) interferometer [9] - and our code and analytic treatment. All of this will eventually permit full system studies of light-ion ICF transport schemes.

It is a pleasure to acknowledge many helpful discussions with Mike Cuneo at Sandia and Peter Hoppe at FZK.

This work is supported by the US Department of Energy through Sandia National Laboratories.

### References

- [1] J. P. Quintenz et al, these proceedings.
- [2] C. L. Olson, et al, Laser Interaction and Related Phenomena, 557 (1994).
- [3] M. P. Desjarlais, Phys. Fluids **B1**, 1709 (1989).
- [4] J. P. Quintenz, Sandia National Laboratories, private communication.
- [5] see for example H. Laqua, H. Bluhm, L. Buth, and P. Hoppe, Jour. Appl. Phys. **77**, 5545 (1995), and references therein.
- [6] W. A. Noonan, T. G. Jones, and P. F. Ottinger, Rev. Sci. Inst., accepted for publication.
- [7] B. V. Oliver, P. F. Ottinger, and D. V. Rose, Phys. Plasmas, accepted for publication.
- [8] D. R. Welch, M. E. Cuneo, C. L. Olson, and T. A. Melhorn, Phys. Plasmas **3**, 2113 (1996)
- [9] B. V. Oliver and R. N. Sudan, BEAMS 92 conf. proceedings (1992), p.921.
- [10] B. V. Weber and S. F. Fulghum, Rev. Sci. Inst., accepted for publication.